Published in final edited form as:
Biochim Biophys Acta. 2007 June ; 1768(6): 1454–1465.

Physical properties of the lipid bilayer membrane made of calf lens lipids: EPR spin labeling studies

Justyna Widomska[a], **Marija Raguz**[a], **James Dillon**[b], **Elizabeth R. Gaillard**[c], and **Witold K. Subczynski**[a,*]

a*Department of Biophysics, Medical College of Wisconsin, Milwaukee, Wisconsin 53226, USA*

b*Department of Ophthalmology, Columbia University, New York, New York 10032, USA*

c*Department of Chemistry and Biochemistry, Northern Illinois University, DeKalb, Illinois, 60115, USA*

Abstract

The physical properties of a membrane derived from the total lipids of a calf lens were investigated using EPR spin labeling and were compared with the properties of membranes made of an equimolar 1-palmitoyl-2-oleoylphosphatidylcholine/cholesterol (POPC/Chol) mixture and of pure POPC. Conventional EPR spectra and saturation-recovery curves show that spin labels detect a single homogenous environment in all three membranes. Profiles of the order parameter, hydrophobicity, and oxygen transport parameter are practically identical in lens lipid and POPC/Chol membranes, but differ drastically from profiles in pure POPC membranes. In both lens lipid and POPC/Chol membranes, the lipids are strongly immobilized at all depths, which is in contrast to the high fluidity of the POPC membrane. Hydrophobicity and oxygen transport parameter profiles in lens lipid and POPC/Chol membranes have a rectangular shape with an abrupt change between the C9 and C10 positions, which is approximately where the steroid ring structure of cholesterol reaches into the membrane. At this position, hydrophobicity increases from the level of methanol to the level of hexane, and the oxygen transport parameter increases by a factor of 2-3. These profiles in POPC membranes are bell-shaped. It is concluded that the high level of cholesterol in lens lipids makes the membrane stable, immobile, and impermeable to both polar and nonpolar molecules.

Keywords

lens lipids; calf; oxygen transport; cholesterol; membrane; EPR

1. Introduction

The fiber cell plasma membrane of the eye lens is an interesting and intriguing biological system with respect to its physical properties and its lateral organization in terms of coexisting membrane domains. To prevent excessive light scattering and compromised lens transparency, fiber cells lose all subcellular organelles during maturation. In fact, the plasma membrane becomes essentially the only supramolecular structure of the adult lens [1]. To maintain its physiological functions, the plasma membrane of the fiber cell has unique biochemical characteristics. In humans, the cholesterol level of the fiber cell plasma membrane is extremely

*__CORRESPONDING AUTHOR__: Witold K. Subczynski, Department of Biophysics, Medical College of Wisconsin, 8701 Watertown Plank Road, Milwaukee, WI 53226, USA, Tel: (414) 456 4038, Fax: (414) 456 6512, E-mail: subczyn@mcw.edu

high, showing cholesterol-to-phospholipid mole ratios from 1 to 2 in the cortex of the lens to as high as 3 to 4 in the lens nucleus, which indicates that during aging the cholesterol-to-phospholipid ratio increases [2,3,4]. This membrane contains more than 50% sphingomyelin and sphingomyelin derivatives [5,6,7] and only trace amounts of polyunsaturated fatty acids [8,9]. It has already been established that a major intrinsic protein (MIP26) is inserted into the membrane during fiber cell development and that aged cell membranes are dense with MIP26 [10]. Additionally, it also has been shown that in a cataractous fiber cell membrane, the level of sphingomyelin is elevated, which may lead to the formation of raft domains [11]. Thus, both in aged and cataractous fiber cells, conditions favor the formation of membrane raft domains.

The fiber cell plasma membrane possesses another interesting feature: at elevated concentration, cholesterol forms immiscible cholesterol crystalline domains within the lipid bilayer [12,13]. These domains were also observed within the plasma membrane of fiber cells from the human eye, where they are essential for normal functioning of the eye and maintain lens transparency to visible light [14,15,16]. It is also suggested that these domains interfere with cataractogenic aggregation of a soluble lens protein, α-crystallin, at the membrane surface [15]. This aggregation is an important feature of the human cataract [17,18] and cataract in animals [19]. Recently, detergent-resistant membranes (DRM, raft domains) were isolated from cortical and nuclear fiber cells of clear lenses of the human eye [20]. The isolated cortical and nuclear rafts exhibit an extremely high cholesterol-to-phospholipid molar ratio, nearly 7. Surprisingly, raft domains could not be isolated from cataractous membranes [20]. It is suggested that the strong binding of insoluble α-crystallin to membranes increases the density of these clusters, forcing them to sediment from the low-density fraction (DRM). It should be noted here that in membranes overloaded with cholesterol, all lipids should be in the liquid-ordered phase, and the entire membrane should be organized as in the raft domain (see also review [21]).

In the present study, we are particularly interested in how lipids are organized in the lipid bilayer portion of the fiber cell plasma membrane. The molecular organization and dynamics have been investigated in the ps-to-μs regime using various spin-labeling techniques. We have studied 1) the alkyl chain order in the 100 ns time regime, 2) the hydrophobicity profile across the membrane, and 3) the local diffusion-solubility characteristics of oxygen molecules (oxygen transport parameter) in the membrane, which are sensitive to molecular dynamics up to 100 μs.

For these studies, we chose the fiber cell plasma membrane from the calf eye lens because it is readily available. The physical properties of the lipid bilayer membranes (liposomes) made of the total lipid extract from the fiber cell plasma membrane of a calf eye lens have been investigated using different EPR approaches. We proposed a lipid bilayer consisting of an equimolar binary mixture of 1-palmitoyl-2-oleoylphosphatidylcholine/cholesterol (POPC/Chol) as a simple model of the calf lens fiber cell plasma membrane. This model was chosen based on the fact that the cholesterol-to-phospholipid ratio in bovine (calf) lens lipids is close to one [22,23,24,25]. Additionally, the bovine (calf) lens fatty acid content consist of ∼33% from C16:0 and ∼34% from C18:1. The other fatty acid abundant in the human lens lipids, C24:1, is represented only by ∼7% in bovine lens fatty acids, although it is the third most abundant fatty acid in this membrane [9,24,26,27]. The most abundant phospholipid in the calf lens membrane is PC (∼32%), which is about 15 times greater than that found in the human lens [9,28], while dihydrosphingomyelin, which is the most abundant phospholipid in the human lens (∼50%), only represents ∼5% in the calf lens membrane [7,29]. The main goal of the present work is to investigate the physical properties of the alkyl chain region of the lipid bilayer made of calf lens lipids. For this reason, we chose only PC with C16:0 and C18:1 fatty acids (POPC) as a good representation of phospholipids for a calf lens membrane. We think that our model (POPC/Chol = 1/1), which reflects the basic fatty acid composition and

cholesterol content of the calf lens membrane, should also reflect the basic physical properties of the lipid bilayer membrane made of calf lens lipids. Additionally, to better elucidate the major factors that determine membrane structure, properties, and organization, we compared results obtained for the above-mentioned membranes with those obtained by us earlier for the pure POPC bilayer [30,31]. We are aware that the phospholipid compositions of the bovine cortex and nucleus are different [29], but as a first approximation in our investigations of the alkyl chain region of the membrane, we have used the total lipid extract from the calf lens. There are no reports in the literature concerning the fatty acid composition of the calf lens cortex and nucleus; however, in humans, this composition is not much different between these two regions and is represented roughly by one third of C16:0, one-third of C18:1, and one-third of C24:1 [2,9]. It should be noted that the human lens phospholipid composition changes significantly with age and cataract, resulting in changes in membrane hydrocarbon chain order [7].

The results reported here for simple membrane systems contribute to an understanding of the organization of the lipid bilayer portion of the native fiber cell plasma membrane to a limited extent. We are aware that a native membrane is dense with intrinsic proteins, and a large portion of lipids is in contact with these proteins, forming boundary lipid and/or trapped lipid domains [32]. Also, in native membranes, cations can affect the organization of lens lipid head group and interface regions [33,34].

This paper also presents the methodological basis for further investigations of the structure and dynamics of the fiber cell plasma membrane of the human eye lens.

Materials and methods

2.1. Materials

POPC, cholesterol and phospholipid spin labels (1-palmitoyl-2-(n-doxylstearoyl) phosphatidylcholine (n-PC, where n = 5, 7, 10, 12, 14, or 16)), and tempocholine-1-palmitoyl-2-oleoylphosphatidic acid ester (T-PC)) were obtained from Avanti Polar Lipids, Inc. (Alabaster, AL). Doxylstearic acid spin labels (n-SASL, where n = 9) and androstane spin labels (ASL) were purchased from Molecular Probes (Eugene, OR). Other chemicals, at least of reagent grade, were purchased from Aldrich (Milwaukee, WI). Chemical structures of lipids and spin labels, as well as their approximate localization in the lipid bilayer membrane, are presented in Fig. 1.

2.2. Isolation of the total lipids from the fiber cell plasma membrane of the calf eye lens

The total lipids from the fiber cell plasma membrane of the calf eye lens were extracted based on minor modifications of the Folch procedure [35]. Fresh calf eyes from animals less than six months old were obtained on the day of slaughter from Brown Packing Company (South Holland, IL). The eyes were dissected and the lenses from ca. 50 eyes were pooled together. The lenses were gently mashed in a 500 mL Erlenmeyer flask with the pestle from a tissue homogenizer to which ca. 200 mL of methanol/chloroform (2:1 v:v) mixture was added, and the slurry was stirred for 30 minutes. The sample was distributed to corex centrifuge tubes and centrifuged at 5000 rpm for 30 minutes. The supernatants were poured into a separatory funnel, and water and methanol were added so that the final ratio of methanol/chloroform/water was 1:2:1 (v:v). The chloroform layer was removed and the water layer was extracted two more times with chloroform. All of the chloroform layers were pooled, dried with $MgSO_4$, filtered, and the solvent was removed. The resultant lipid sample was a soft, white solid stored at −20° C.

2.3. Preparation of lipid bilayer membranes

The membranes used in this work were multilameller dispersions (multilamellar liposomes) made of the appropriate lipids (the total lipid extract from fiber cell plasma membranes of calf eye lenses, the equimolar binary mixture of 1-palmitoyl-2-oleoylphosphatidylcholine/cholesterol (POPC/Chol), and of the pure POPC) containing 1 mol% spin label. The membranes were prepared by the following method [36]: Chloroform solutions of lipids and n-PC or n-SASL were mixed (containing $\sim 0.5 \times 10^{-5}$ mol of total lipids - for brevity we assumed the average molecular weight of lipids in the total lipid extract from eye lens to be 1000 Da), the chloroform evaporated with a stream of nitrogen gas, and the lipid film on the bottom of the test tube thoroughly dried under reduced pressure (about 0.1 mmHg) for 12 h. A buffer solution (0.25 mL of 10 mM PIPES and 150 mM NaCl, pH 7.0) was added to the dried lipids at 40°C and vortexed vigorously. The buffer used for the study of samples with 9-SASL was 0.1 M borate at pH 9.5. A rather high pH was chosen in this case to ensure that all SASL probe carboxyl groups were ionized in the POPC membranes [37].

2.4. Conventional EPR

The membranes (multilamellar liposomes) were centrifuged briefly, and the loose pellet (about 20% lipids, w/w) was used for EPR measurements. For conventional EPR measurements, the sample was placed in a 0.6 mm i.d. capillary made of gas-permeable methylpentene polymer, called TPX, and the capillary was placed inside the EPR dewar insert. It was then equilibrated with nitrogen gas used for temperature control [38,39]. The sample was thoroughly deoxygenated. A Bruker EMX X-band spectrometer with temperature control accessories was used to record the EPR spectra. Modulation amplitude of 1.0 G and an incident microwave power of 5.0 mW were used. EPR spectra were recorded for the temperature range 15 - 45°C. To measure the hydrophobicity profiles across the membrane, hyperfine interactions of nitroxide were used; the sample was frozen (−163°C) and the EPR spectra were recorded with modulation amplitude of 2 G [40]. This was necessary to distinguish the solvent polarity effects from the motional effects on the spectrum. The magnetic parameters (including the hyperfine interactions) of spin labels in the membrane at low temperatures correlate well with those at physiological temperatures [41]. Also, the accessibility of an ion into various parts of the membrane at a physiological temperature is in a good correlation with the hydrophobicity profiles obtained for frozen samples [40,42]. Hydrophobicity profiles obtained for frozen solutions [40,42] are in principal agreement with profiles obtained at physiological temperatures with the use of the isotropic hyperfine constant as a hydrophobicity parameter [43,44]. However, the method of estimating the isotropic hyperfine constant has to be changed for different n-PCs and n-SASLs, which can create artificial discontinuities in the hydrophobicity profiles and make the obtained hydrophobicity profiles less reliable.

2.5. Saturation–recovery EPR

The T_1s of the spin-labels were determined by analyzing the saturation-recovery signal of the central line obtained by short-pulse saturation-recovery EPR at X-band [45,46,47]. The saturation-recovery spectrometer was described previously [47,48]. For saturation-recovery measurements, the sample was placed in a capillary (i.d. = 0.6 mm) made of a gas-permeable methylpentene polymer, TPX [38,39]. A relatively low level of observing power (8 μW, with the loop-gap resonator delivering an H_1 field of 3.6×10^{-5} gauss) was used for all experiments to avoid microwave power saturation (which induces artificial shortening of the apparent T_1). Accumulations of the decay signals were carried out with 2048 data points on each decay. For measurements of the oxygen transport parameter, the concentration of oxygen in the sample was controlled by equilibration with the same gas that was used for the temperature control (i.e., a controlled mixture of nitrogen and dry air adjusted with flowmeters (Matheson Gas Products model 7631H-604)) [38,39,49].

To monitor the local diffusion-solubility characteristics of oxygen molecules in the membrane, the bimolecular collision rate between oxygen (a fast relaxing species) and the nitroxide spin-label (a slow relaxing species) placed at specific locations in the membrane was evaluated in terms of an oxygen transport parameter (W(x)). W(x) was defined as

$$W(\mathrm{x}) = T_1^{-1}(\mathrm{air},\ \mathrm{x}) - T_1^{-1}(\mathrm{N}_2,\ \mathrm{x}), \tag{1}$$

where the T_1s are the spin-lattice relaxation times of the nitroxide in samples equilibrated with atmospheric air and nitrogen, respectively [45,49]. W(x) is proportional to the product of local translational diffusion coefficient D(x) and the local concentration C(x) of oxygen at a "depth" x in a lipid bilayer that is equilibrated in the atmospheric air:

$$W(\mathrm{x}) = AD(\mathrm{x})C(\mathrm{x}), \quad A = 8\pi p r_0, \tag{2}$$

where r_0 (about 4.5 Å) is the interaction distance between oxygen and the nitroxide radical spin-label [50,51], and p is the probability that an observable event occurs when a collision does occur and is very close to one [38,52,53].

3. Results and discussion

3.1. Conventional EPR spectra indicate the presence of a single lipid environment on the time scale of 10^{-7}s

EPR spectra were recorded at different temperatures (from 15 to 45°C) and different depths in the membranes (from the polar headgroup region with T-PC to the membrane center with 14- and 16-PC). Figure 2 shows a panel of conventional EPR spectra of 5-, 10-, and 16-PC in investigated membranes at 35°C.

There are two remarkable features of these spectra: the similarities between the spectra obtained for membranes made of the total lipid extract from the fiber cell plasma membrane and the equimolar POPC/Chol mixture, and the striking differences of spectra obtained for pure POPC membranes. There is no indication of the presence of two components in the EPR spectra at any temperature and at any depth in the membrane for all of the samples. The former feature confirms that our simple model (membrane made of POPC/Chol mixture) should, in good approximation, reflect the physical properties of the membrane made of the total lipid extract from the fiber cell plasma membrane (see also other similarities indicated below). The latter feature is consistent with the oxygen transport data, in which all saturation-recovery curves were single-exponential curves. We acknowledge that it is difficult to unambiguously demonstrate the absence of a second component (strongly immobilized component) in conventional EPR spectra. Previously, we showed that W(x) is a better parameter for distinguishing different membrane domains (discrimination by oxygen transport – the DOT method) when the lifetime of domains is longer than $W(\mathrm{x})^{-1}$ [32,46,54]. As described below, W(x) did not show any signs of the presence of two membrane domains.

3.2. Alkyl chain order

The hydrocarbon chain order was studied at seven depths (5-, 7-, 10-, 12-, 14-, 16-PC, and 9-SASL) in the membranes. Figure 3 shows the profiles of the order parameter obtained in these membranes at 35°C. The order parameter, S, was calculated using the equation

$$S = 0.5407(A'_{\mathrm{II}} - A'_{\perp}) / a_0 \tag{3}$$

Where

$$a_0 = \left(A'_{II} + 2A'_{\perp}\right) / 3 \quad (4)$$

A'_{II} and $A'_{\perp}$ were measured directly from the EPR spectra as indicated in Fig. 2 [55]. The order parameter at the *n*th position reflects the distribution of vector $C_{n-1} \rightarrow C_{n+1}$ along the molecular axis. The alkyl chain order decreases gradually with an increase of depth in the membrane. The lipid bilayer made of the lens lipids is only slightly less ordered than the membrane made of the equimolar mixture of POPC/Chol, while both membranes are considerably more ordered at all depths than the pure POPC bilayer.

Figure 4 shows the alkyl chain order displayed as a function of temperature. With an increase in temperature, the alkyl chain order decreases. These data strongly indicate that the order parameters measured at the same depths in the lipid bilayer made of the total lipid extract from the fiber cells and in the membrane made of the equimolar mixture of POPC/Chol are similar in the wide range of temperature (15 - 45°C). Additionally, the order parameter in these two membranes very weakly depends on temperature. In contrast, in the POPC bilayer, the change in the order parameter with temperature is significant (see Fig. 7 in Ref. [30]). Because of this dependence, the differences in the order parameter profiles are enhanced at lower temperatures. Our observations are in agreement with measurements of the fluorescence anisotropy in human [56] and bovine [57] lens fibers as a function of temperature, which also demonstrate a weak dependence on temperature.

Our results are consistent with the strong lipid immobilization reported for the fiber cell plasma membrane [56,57,58,59] and indicate that the high cholesterol content is responsible for high order and strong lipid immobilization of the fiber cell plasma membrane. In native lens membranes and reconstituted lens lipid membranes, the head group interactions, especially between sphingolipids, would be expected to increase rigidity and immobilize the lipids [60, 61,62,63]. Our data illustrate the effect of cholesterol as “a buffer of membrane fluidity” not only in small changes of the order parameter with temperature, but also in the small differences at different depths in the membrane. The ability to buffer the membrane fluidity is likely to be a property unique to cholesterol because the other membrane modifiers, like dipolar carotenoids [64,65] and transmembrane α-helical peptides, with smooth [30] and rough [31] hydrophobic peptide surfaces increase the order of the POPC membrane but do not decrease gradients of the order parameter created by changing temperature or the position within the lipid bilayer. We would like to comment here that the effects of cholesterol on ordering and immobilization of lipids are very strong in saturated membranes [36,66,67]. Unsaturated alkyl chains greatly reduce these effects [33,66,68,69]. Thus, high content of saturated lipids in eye lens membranes should enhance the ordering effect of cholesterol (for more discussion, see review [70]).

3.3. Hydrophobicity profiles across membranes

EPR spectra of n-PCs, where n = 5, 7, 10, 12, 14, 16, T-PC, and 9-SASL in frozen suspensions of lipid bilayer membranes consisting of the total lipid extract from fiber cell plasma membranes, equimolar POPC/Chol mixture, and pure POPC, lacked any sign of the presence of the two components. Therefore, A_Z values can be simply determined from the EPR spectra as shown in Fig. 5. As mentioned above, the similarities between the spectra obtained for membranes made of the total lipid extract from the fiber cell plasma membrane and the equimolar POPC/Chol mixture, and their differences with spectra for pure POPC membranes are evident. Figure 6 shows hydrophobicity profiles across these membranes. Here, the $2A_Z$ data are presented as a function of the approximate position of the nitroxide moiety of the spin label within the lipid bilayer. Smaller $2A_Z$ values (upward changes in the profiles) indicate higher hydrophobicity [30,31,40]. The width of the hydrocarbon phase and the locations of the nitroxide moiety in the stearic acid chain are simply scaled to the number of carbon atoms in

the hydrocarbon chain. Based on the fatty acid composition of the calf lens membranes, we assume that the thickness of the lipid bilayer made of the total lipid extract from the fiber cells is the same as POPC/Chol membranes. As was shown earlier, longer alkyl chains simply make the central hydrophobic regions wider without increasing hydrophobicity at the bilayer center [40].

For membranes made of the total lipid extract from the fiber cell plasma membrane and the equimolar POPC/Chol mixture, the hydrophobicity profiles show a very similar rectangular shape, with an abrupt increase of hydrophobicity between C9 and C10 from the level of methanol to a level close to pure hexane. We relate the local hydrophobicity as observed by $2A_Z$ to the hydrophobicity (or ε) of the bulk organic solvent by referring to Fig. 2 in Ref. [40]. Each hydrophobicity profile differs significantly from that of a pure POPC membrane that has a typical bell-like shape with a gradual increase of hydrophobicity toward the bilayer center (see Fig. 10 in Ref. [31]). It should be pointed out that the rectangular shape of the hydrophobicity profiles is characteristic for both saturated and unsaturated membranes with a high cholesterol content [40].

The striking similarity of the profiles presented in Figs. 6A and B, as well as the lipid composition of the fiber cell plasma membrane, permits the assumption that the high cholesterol content is responsible for the unique shape of the hydrophobicity profile across the lens lipid membrane. Four remarkable features of this profile should be emphasized: 1) high polarity of both the polar headgroup region and the hydrocarbon region to the depth of the ninth carbon; 2) high hydrophobicity in the central region of the bilayer, which is deeper than the ninth carbon (the hydrophobicity reaches the level of hexane; 3) sharp increases in hydrophobicity at the ninth carbon, which is about where the bulky, rigid steroid ring structure of cholesterol reaches into the membranes [71] (the transition point for the lens membrane is observed at the same depth as for EYPC/Chol = 1/1 membranes (approximately 70% of EYPC is POPC [72]), deeper than for saturated PC membranes containing 50 mol% cholesterol, and more shallow than for DPPC/Chol = 1/1 membranes [40]); and 4) the $2A_Z$ values are almost constant inside the sharp transition points in the profile. The values lie somewhat lower than $2A_Z$ values for saturated and unsaturated PC membranes containing 30 mol% cholesterol, which agrees with the observation that increases in cholesterol content above 30 mol% causes slight decreases in hydrophobicity of the membrane center [40].

3.4. Saturation recovery measurements

Figure 7 shows typical saturation-recovery curves for 5- PC in the membranes at 35°C in the presence and absence of oxygen. The recovery curves were fitted by single, double, and triple exponentials and compared. The results indicate that for all of the recovery curves obtained in this work, no substantial improvement in the fitting was observed when the number of exponentials was increased from one, suggesting that these recovery curves can be analyzed as single exponentials. The decay time constants were determined within an accuracy of +/−3%.

Saturation-recovery measurements were carried out systematically as a function of the partial pressure of oxygen in the equilibrating gas mixture, the location of spin labels in the membrane, and within the temperature range of 15 - 45°C. Previously, we proved that lipid spin labels are able to partition between different membrane domains, including: bulk lipid and trapped lipid domains in membranes dense with integral membrane proteins [32], bulk lipid and raft domains in raft forming mixtures [73,74], bulk lipids and rafts in the influenza virus membrane [46], and liquid-disordered and liquid-ordered domains in DMPC/Chol membranes [75]. We also found that the presence of two recovery constants (i.e., the presence of two membrane environments) can be observed more readily in the presence of oxygen [32,46]. However, in this work, single exponential recovery was consistently observed. This indicates the presence

of a single homogenous membrane when averaged over 0.4 μs (the shortest recovery time observed here), and that, in these membranes, the rates of lipid exchange among the purported membrane domains is greater than the T_1 relaxation rate (greater than 2.5×10^6 s^{-1}, see Ref. [46] for more detail).

3.5. Saturation-recovery measurements of the oxygen transport parameter

In Fig. 8,T_1^{-1} values measured at a fixed depth (for 5-, 10-, and 16-PC) in the lens lipid membranes at 25°C are plotted as a function of oxygen concentration (in % air) in the equilibrating gas mixture. All plots of T_1^{-1} for investigated membranes show a linear dependence on the oxygen concentration between 0 and 50% air for a temperature region between 15 and 45°C for all spin labels. At each depth, the oxygen transport parameter was obtained by extrapolating the linear plot to the sample equilibrated with atmospheric air (100% air, see Eq. (1)) as shown in Fig. 8. This process is required because accurate observation of saturation recovery becomes increasingly difficult as the oxygen partial pressure is increased due to fast relaxations. A minimum of than three decay measurements were performed for each point in the plot with accuracy of the evaluation of W(x) better than +/−10%. W(x) values are displayed in Fig. 9.

Even in the presence of molecular oxygen (when the bimolecular collision rate between molecular oxygen and the nitroxide moiety of the spin label is much greater than T_1^{-1} in the absence of oxygen), all saturation-recovery curves could be fitted to a single exponential function. In earlier work on the fluid-phase membrane made of DMPC/cholesterol mixture [75], in the absence of oxygen, all recoveries followed single-exponential functions. In the presence of oxygen, double exponential recoveries were observed for cholesterol concentrations at which liquid-ordered and liquid-disordered phases coexist (see phase diagram in [76]). This indicates that the oxygen transport parameter can discriminate coexisting phases (domains, see also Refs. [32,46,75]) and that molecular oxygen makes a particularly useful probe for studies of the lateral organization of lipid bilayer membranes.

The single exponential recoveries indicate that the lipid environment is homogenous in terms of oxygen transport in the microsecond range as defined by T_1 in all three investigated membranes. The pure POPC membrane and the membrane made of the POPC/Chol = 1/1 mixture should form the sole liquid-disordered and liquid-ordered phases, respectively [77]. However, for the membrane made of the total lipid extract from the fiber cell plasma membranes, the presence of two lipid environments could be in principle expected: the liquid-ordered phase region (raft domain) and the bulk lipid region in which lipids are organized as in the liquid-disordered phase. In a similar experiment, the conventional EPR spectra from lipid spin labels incorporated into the plasma membrane vesicles of RBL-2H3 cells showed the presence of two coexisting phases, liquid-ordered-like and liquid-disordered-like [78]. However, EPR spectra of the same spin labels in vesicles made of the total lipid extract from the plasma membrane showed only the liquid-ordered-like phase. No components of the liquid-disordered-like phase could be resolved in these lipid extracts. The authors concluded that membrane-associated proteins are important for the coexistence of liquid-ordered-like and liquid-disordered-like regions in the plasma membranes. Thus, in native membranes, proteins are often the driving force for the lateral phase separation of lipids [79].

It is important to note that in membranes overloaded with cholesterol all lipids should be in the liquid-ordered phase (see Ref. [21]). These conditions exist in the human fiber cell plasma membrane where the cholesterol-to-phospholipids mole ratio is extremely high, from 1 to as high as 4 [2,3]. In these conditions, the entire lipid bilayer is not only saturated with cholesterol, which shows a threshold of solubility in the phospholipid bilayers of about 50 mol% [80], but also the immiscible cholesterol crystalline domains are formed within the model lipid bilayer membranes [12,13] and within the lipid bilayer portion of the fiber cell plasma membrane

[14-17]. Given these restrictions, we also investigated whether or not immiscible cholesterol crystalline domains are formed within the lipid bilayer made of the calf lens lipids. The spin-labeled cholesterol analogue, androstane spin label (ASL, see Fig. 1), was used for this experiment. It should approximate the distribution of cholesterol molecules in the membrane because of the overall similarity of ASL and cholesterol molecular structures as well as the similarity of the phase diagrams of membranes with and without spin label [81,82]. Additionally, we have previously observed that ASL can identify the existence of pure cholesterol crystalline domains in DMPC/Chol = 1/2 and POPC/Chol = 1/2 membranes. In these membranes, clear double exponential saturation recovery signals were observed in the presence of oxygen (data not shown), which indicates that ASL is located in two environments with different oxygen transport rates, which we attributed to the liquid-ordered and cholesterol crystalline domains. Phospholipid spin labels, which should not partition into the cholesterol crystallites (pure cholesterol domains), cannot discriminate these domains.

When ASL is added to the membrane made of the total lipid extract from fiber cells, only single exponential saturation recovery signals both in the absence and in the presence of molecular oxygen are observed. As expected, the cholesterol crystalline domain is not formed in this membrane, presumably because the cholesterol content is too low [23,24,28]. The values of the oxygen transport parameter are very similar to those obtained with ASL in the liquid-ordered domain for membranes overloaded with cholesterol (made of POPC/Chol 1/2 mixture). It supports our conclusion that properties of the membrane made of calf lens lipids are similar to properties of POPC bilayer containing 50 mol% cholesterol. Additionally, values of the oxygen transport parameter obtained with ASL in membranes made of lens lipids are practically the same as values obtained with 10-PC (Fig. 10). This confirms that the bulky, rigid steroid ring structure of cholesterol reaches into the membrane to the depth of the ninth carbon because the nitroxide fragment of ASL is located just below the steroid ring structure (see Fig. 1).

3.6. Profiles of the oxygen transport parameter

The membrane profiles of the oxygen transport parameter at 15, 25, and 35°C were obtained using eight lipid spin labels shown in Fig. 1. These profiles for lipid bilayer membranes made from the lens lipids and POPC/Chol mixture are presented in Fig. 9. The profiles for the membrane made from the lens lipids (Fig. 9A) have a remarkable feature - their rectangular shape, with an abrupt increase of the oxygen transport parameter between the C9 and C10 position. The abrupt increase is as large as 2-3 times, and the overall change of the oxygen transport parameter across the membrane becomes as large as ~5 times. The oxygen transport parameter from the membrane surface to the depth of the ninth carbon is as low as in gel-phase PC membranes, and at locations deeper than the ninth carbon, as high as in fluid-phase PC membranes [45,83]. These results also indicate that with the use of the saturation-recovery EPR technique and lipid spin labels the main features of the profile could be obtained practically at the atomic resolution.

Profiles for the membrane made of the lens lipids (Fig. 9A) are almost identical to those for the liquid-ordered-phase membrane made from the equimolar mixture of unsaturated POPC and cholesterol (Fig. 9B), and those for the liquid-ordered-phase membrane made from the equimolar mixture of saturated DMPC and cholesterol [75]. However, these profiles present a marked contrast with typical bell-shaped profiles for the liquid-disordered-phase unsaturated POPC (see Fig. 4 in Ref. [31])) and saturated DMPC [75] membranes in the absence of cholesterol for which the oxygen transport parameter increases monotonically toward the membrane center without any abrupt changes. Thus, we can conclude that the unique properties of the membrane made from equimolar POPC/Chol mixture, as well as the membrane made from lens lipids, are determined by the high cholesterol content. This conclusion is supported

by the fact that the abrupt increase in the oxygen transport parameter occurs at the depth at which the rigid tetracyclic cholesterol structure is immersed [71,75].

One unexpected finding is that the change from the gel phase-like membrane to the liquid crystalline-like membrane occurs within the distance of one carbon atom on the alkyl chain. This transition is smooth for membranes without cholesterol or membranes containing a small concentration of cholesterol [30,31,45,75,83]. It indicates that cholesterol at high content decreases the fluidity of the membrane region close to the membrane surface to the level of gel phase and increases it in the membrane center to the level of pure liquid-crystalline bilayer. In addition, high cholesterol content decreases the vertical fluctuations (budding) of all membrane components, so that the rigid plate-like portion of all cholesterol molecules are aligned at the same depth of the ninth carbon in the alkyl chains. Similar profiles were presented in Fig. 6 for membranes made from lens lipids and the POPC/Chol mixture containing 50 mol % cholesterol when membrane hydrophobicity was plotted as a function of depth. For these membranes, hydrophobicity increases within the same distance of one carbon atom on the alkyl chain from the level of methanol to the level of pure hexane. Similar hydrophobicity profiles were also obtained for other saturated and unsaturated membranes containing 50 mol% cholesterol [40]. Hydrophobicity measurements were performed at −163°C when vertical fluctuations were frozen. To explain the rectangular oxygen transport parameter profiles (Fig. 9A and B), we should consider localization of cholesterol in the lipid bilayer membrane. The molecule of cholesterol is located in one leaflet of the bilayer, and its rigid plate-like portion extends to a depth of the ninth carbon atom in the lipid alkyl chains [71]. The cross-section of the isooctyl chain of the cholesterol molecule is much smaller than the cross-section of the rigid steroid ring and, therefore, produces additional possibilities for undulations and *trans-gauche* transitions of alkyl chains in the membrane center. It follows that the alkyl chains and cholesterol rigid plate-like portions are closely packed to the depth of the ninth carbon, with few vacant pockets to allow entrance and movement of even small molecules such as molecular oxygen. Mismatch of cross-sections at different positions of the cholesterol molecule creates many vacant pockets in the membrane center that oxygen molecules can occupy, jumping from one pocket to an adjacent one or moving with the movement of the pocket itself due to the rapid *gauche-trans* isomerization of the phospholipid hydrocarbon chains. Other membrane modifiers, dipolar carotenoids [84] and transmembrane α-helical peptides [30,31], decrease the oxygen transport parameter at all depths; their effects are strongest in the membrane center. These modifiers have a rigid structure, the same cross-section at all depths, and span the entire lipid bilayer. Bacteriorhodopsin makes the profile completely flat [32].

It is important to comment on an apparent discrepancy between the observations that cholesterol increases an oxygen transport rate in the membrane center (see profiles of the oxygen transport parameter in Fig. 9A and B), and the well-established condensing [85,86] and ordering [67] effects of cholesterol, which extend to the whole alkyl chain of the lipid bilayer (see also profiles of the order parameter presented in Fig. 3). It is pertinent that the order parameter indicates a static property of the lipid bilayer, whereas the collisions between molecular oxygen and the nitroxide moiety of spin labels (oxygen transport parameter) characterize membrane dynamics. Moreover, deviations in the alkyl chain segment direction from the bilayer normal accumulate as one proceeds from the bilayer surface to the membrane interior, a result of the effective tethering of the alkyl chain at the bilayer surface. Consequently, ordering of the alkyl chain induced by steric contact with the plate-like portion of cholesterol will also cause ordering of the distal fragment of the alkyl chain, even though the number of *gauche* bonds is unchanged in that fragment. Therefore, the increased mobility induced by cholesterol in the membrane center, indicated by dynamic spectroscopic characteristics, is not inconsistent with increased order, a static membrane property (see also Ref. [47]).

4. Conclusions

Our observations from conventional and saturation-recovery EPR measurements on membranes from calf lens lipids suggest that the lipid exchange rates among possible membrane domains are fast, and the domains, if they exist, must be forming and dispersing rapidly on a time scale shorter than 0.4 μs. Also, the immiscible cholesterol crystalline domains are not detected with the cholesterol analogue spin label.

The lipids of these membranes are strongly immobilized, showing a high order parameter at all depths across the lipid bilayer with a very weak dependence on temperature.

The hydrophobicity profiles for the membrane made of the lens lipids correlate well with those obtained in this work and previously for membranes with high (50 mol%) cholesterol content. These results indicate that the peak hydrophobicity in the center of the membrane is a hydrophobic barrier to permeation of small polar molecules, including water.

Similarly, the profiles of the oxygen transport parameter for membranes made of the lens lipids correlate well with those for membranes with high (50 mol%) cholesterol content. These results indicate that the rigidity barrier, which is more significant for permeation of nonpolar molecules (including molecular oxygen), is located in the polar headgroup and near-surface regions of the lipid membrane.

The results obtained in this work indicate that the high cholesterol content in the total lipid extract from the fiber cell plasma membrane is responsible for these unique properties of the membrane and allow us to conclude that the entire membrane is in the liquid-ordered-like phase.

Acknowledgements

This work was supported by grants EY015526, EB002052, and EB001980 of the National Institute of Health.

References

1. Rafferty, NS. Lens morphology. In: Maisel, H., editor. The Ocular Lens: Structure, Function and Pathology. Marcel Dekker; New York: 1985. p. 1-60.
2. Li LK, So L, Spector A. Membrane cholesterol and phospholipids in consecutive concentric sections of human lenses. J Lipid Res 1985;26:600–609. [PubMed: 4020298]
3. Li LK, So L, Spector A. Age-dependent changes in the distribution and concentration of human lens cholesterol and phospholipids. Biochim Biophys Acta 1987;917:112–120. [PubMed: 3790601]
4. Truscott R. Age-related nuclear cataract: a lens transport problem. Ophthalmic Res 2000;32:185–194. [PubMed: 10971179]
5. Byrdwell WC, Borchman D, Porter RA, Taylor KG, Yappert MC. Separation and characterization of the unknown phospholipids in human lens membranes. Invest Ophthalmol Vis Sci 1994;35:4333–4343. [PubMed: 8002253]
6. Byrdwell WC, Borchman D. Lipid chromatography/mass-spectrometric of sphingomyelin and dihydrosphingomyelin of human lens membranes. Ophthalmic Res 1997;29:191–206. [PubMed: 9261843]
7. Huang L, Grami V, Marrero Y, Tang D, Yappert MC, Rasi V, Borchman D. Human lens phospholipid change with age and cataract. Invest Ophthalmol Vis Sci 2005;46:1682–1689. [PubMed: 15851569]
8. Broekhuyse RM, Soeting WJ. Lipids in tissue of the eye: XV. Essential fatty acids in lens lipids. Exp Eye Res 1976;22:653–657. [PubMed: 776644]
9. Zelenka PS. Phospholipid composition and metabolism in the embryonic chicken lens. Exp Eye Res 1978;26:267–274. [PubMed: 639879]
10. Varadaraj K, Kushmerick C, Baldo GJ, Bassnett S, Shiels A, Mathias RT. The Role of MIP in lens fiber cell membrane transport. J Membrane Biol 1999;170:191–203. [PubMed: 10441663]

11. Yappert MC, Borchman D, Vorobyov I, Rujoi M, DuPre DB. Sphingolipid changes in cataractous lenses. Invest Ophthalmol Vis Sci 2001;42:S539.
12. Bach D, Wachtel E. Phospholipid/cholesterol model membranes: formation of cholesterol crystallites. Biochim Biophys Acta 2003;1610:187–197. [PubMed: 12648773]
13. Mason RP, Tulenko TN, Jacob RF. Direct evidence for cholesterol crystalline domains in biological membranes: role in human pathobiology. Biochim Biophys Acta 2003;1610:198–207. [PubMed: 12648774]
14. Borchman D, Cenedella RJ, Lamba OP. Role of cholesterol in the structural order of lens membrane lipids. Exp Eye Res 1996;62:191–197. [PubMed: 8698079]
15. Jacob RF, Cenedella RJ, Mason RP. Direct evidence for immiscible cholesterol domains in human ocular lens fiber cell plasma membranes. J Biol Chem 1999;274:31613–31618. [PubMed: 10531368]
16. Jacob RF, Cenedella RJ, Mason RP. Evidences for distinct cholesterol domains in fiber cell membranes from cataractous human lenses. J Biol Chem 2001;276:13573–13578. [PubMed: 11278611]
17. Chandrasekher G, Cenedella RJ. Protein association with human lens “native” membrane during aging and cataract formation. Exp Eye Res 1995;60:707–717. [PubMed: 7641853]
18. Cobb BA, Petrash JM. α-crystallin chaperone-like activity and membrane binding in age-related cataracts. Biochemistry 2002;41:483–490. [PubMed: 11781086]
19. Cenedella RJ, Bierkamper GG. Mechanism of cataract production by 3-beta(2-diethylaminoethoxy) androst-5-en-17-one hydrochloride, U18666A: an inhibitor of cholesterol biosynthesis. Exp Eye Res 1979;28:673–688. [PubMed: 467524]
20. Rujoi M, Jin JL, Borchman D, Tang DX, Yappert MC. Isolation and lipid characterization of cholesterol-enriched fractions in cortical and nuclear human lens fibers. Invest Ophthalmol Vis Sci 2003;44:1634–1642. [PubMed: 12657603]
21. Munro S. Lipids rafts: elusive or illusive. Cell 2003;115:377–388. [PubMed: 14622593]
22. Broekhuyse RM, Kuhlmann ED. Lens membrane I. Composition of urea-trated plasma membranes of calf lens. Exp Eye Res 1974;19:297–302. [PubMed: 4417164]
23. Broekhuyse RM, Kuhlmann ED. Lens membrane IV. Preparative isolation and characterization of membranes and various membrane proteins from calf lens. Exp Eye Res 1978;26:305–320. [PubMed: 416964]
24. Broekhuyse RM. Membrane lipids and proteins in ageing lens and cataract. Ciba Foundation Symposium 1973;19:135–149.
25. Roy D, Rosenfeld L, Spector A. Lens plasma membrane: isolation and biochemical characterization. Exp Eye Res 1982;35:113–129. [PubMed: 7151881]
26. Anderson RE, Maude MB, Feldman GL. Lipids of ocular tissues I. The phospholipids of mature rabbit and bovine. Biochim Biophys Acta 1969;187:345–353. [PubMed: 4310714]
27. Broekhuyse RM, Roelfzema H, Breimer ME, Karslon KA. Lipids in tissues of the eye. X. Molecular species of sphingomyelins from different parts of calf lens in relation to differentiation and aging. Exp Eye Res 1974;19:477–484. [PubMed: 4426349]
28. Broekhuyse RM. Phospholipids in tissues of the eye. I. Isolation, characterization and quantitative analysis by two-dimensional thin-layer chromatography of diacyl and vinyl-ether phospholipids. Biochim Biophys Acta 1968;152:307–315. [PubMed: 4296335]
29. Borchman D, Yappert MC, Afzal M. Lens lipids and maximum lifespan. Exp Eye Res 2004;79:761–768. [PubMed: 15642313]
30. Subczynski WK, Lewis RNAH, McElhaney RN, Hodges RS, Hyde JS, Kusumi A. Molecular organization and dynamics of 1-palmitoyl-2-oleoylphosphatidylcholine bilayers containing a transmembrane α-helical peptide. Biochemistry 1998;37:3156–3164. [PubMed: 9485469]
31. Subczynski WK, Pasenkiewicz-Gierula M, McElhaney RN, Hyde JS, Kusumi A. Molecular dynamics of 1-palmitoyl-2-oleoylphosphatidylcholine membranes containing transmembrane α-helical peptides with alternating leucine and alanine residues. Biochemistry 2003;42:3939–3948. [PubMed: 12667085]
32. Ashikawa I, Yin JJ, Subczynski WK, Kouyama T, Hyde JS, Kusumi A. Molecular organization and dynamics in bacteriorhodopsin-rich reconstituted membranes: Discrimination of lipid environments

by the oxygen transport parameter using a pulse ESR spin-labeling technique. Biochemistry 1994;33:4947–4952. [PubMed: 8161556]

33. Rujoi M, Borchman D, DuPre DB, Yappert MC. Interaction of Ca+ with Sphingomyelin and Dihydrosphingomyelin. Biophys J 2002;82:3096–3104. [PubMed: 12023233]
34. Tang D, Borchman D, Yappert MC, Vrensen GFJM, Rasi V. Influence of age, diabetes and cataract on calcium, lipid-calcium, and protein-calcium relationships in human lenses, Invest. Ophthalmol Vis Sci 2003;44:2059–2066.
35. Folch J, Lees M, Sloane Stanley GH. A simple method for the isolation and purification of total lipids from animal tissues. J Biol Chem 1957;226:497–509. [PubMed: 13428781]
36. Kusumi A, Subczynski WK, Pasenkiewicz-Gierula M, Hyde JS, Merkle H. Spin-label studies on phosphatidylcholine-cholesterol membranes: effects of alkyl chain length and unsaturation in the fluid phase. Biochim Biophys Acta 1986;854:307–317. [PubMed: 3002470]
37. Kusumi A, Subczynski WK, Hyde JS. Effects of pH on ESR spectra of stearic acid spin labels in membranes: probing the membrane surface. Fed Proc 1982;41:1394.
38. Hyde, JS.; Subczynski, WK. Spin-label oximetry. In: Berliner, LJ.; Reuben, J., editors. Biological Magnetic Resonance, vol 8, Spin Labeling: Theory and Applications. Plenum Press; New York: 1989. p. 399-425.
39. Subczynski WK, Felix CC, Klug CS, Hyde JS. Concentration by centrifugation for gas exchange EPR oximetry measurements with loop-gap resonators. J Magn Reson 2005;176:244–248. [PubMed: 16040261]
40. Subczynski WK, Wisniewska A, Yin JJ, Hyde JS, Kusumi A. Hydrophobic barriers of lipid bilayer membranes formed by reduction of water penetration by alkyl chain unsaturation and cholesterol. Biochemistry 1994;33:7670–7681. [PubMed: 8011634]
41. Kusumi A, Pasenkiewicz-Gierula M. Rotational diffusion of steroid molecule in phosphatidylcholine membranes: effects of alkyl chain length, unsaturation and cholesterol as studied by a spin-label method. Biochemistry 1988;27:4407–4415. [PubMed: 3166984]
42. Wisniewska A, Subczynski WK. Effects of polar carotenoids on the shape of the hydrophobic barrier of phospholipids bilayer. Biochim Biophys Acta 1998;1368:235–246. [PubMed: 9459601]
43. Marsh D. Polarity and permeation profiles in lipid membranes. Proc Natl Acad Sci USA 2001;98:7777–7782. [PubMed: 11438731]
44. Fretten P, Morris SJ, Watts A, Marsh D. Lipid-lipid and lipid-protein interactions in chromaffin granule membranes: A spin label ESR study. Biochim Biophys Acta 1980;598:247–259. [PubMed: 6246946]
45. Subczynski WK, Hyde JS, Kusumi A. Oxygen permeability of phosphatidylcholine-cholesterol membranes. Proc Natl Acad Sci USA 1989;86:4474–4478. [PubMed: 2543978]
46. Kawasaki K, Yin JJ, Subczynski WK, Hyde JS, Kusumi A. Pulse EPR detection of lipid exchange between protein-rich raft and bulk domains in the membrane: Methodology development and its application to studies of influenza viral membrane. Biophys J 2001;80:738–748. [PubMed: 11159441]
47. Yin JJ, Subczynski WK. Effect of lutein and cholesterol on alkyl chain bending in lipid bilayers: a pulse electron paramagnetic resonance spin labeling study. Biophys J 1996;71:832–839. [PubMed: 8842221]
48. Subczynski WK, Antholine WE, Hyde JS, Kusumi A. Microimmiscibility and three-dimensional dynamic structure of phosphatidylcholine-cholesterol membranes: translational diffusion of copper complex in the membrane. Biochemistry 1990;29:7936–7945. [PubMed: 2261449]
49. Kusumi A, Subczynski WK, Hyde JS. Oxygen transport parameter in membranes as deduced by saturation recovery measurements of spin-lattice relaxation times of spin labels. Proc Natl Acad Sci USA 1982;79:1854–1858. [PubMed: 6952236]
50. Fischkoff S, Vanderkooi JM. Oxygen diffusion in biological and artificial membranes determined by the fluorochrome pyrene. J Gen Physiol 1975;65:663–676. [PubMed: 1176942]
51. Subczynski WK, Hyde JS. The diffusion-concentration product of oxygen in lipid bilayers using the spin-label T1 method. Biochim Biophys Acta 1981;643:283–291. [PubMed: 6261814]
52. Hyde JS, Subczynski WK. Simulation of ESR spectra of the oxygen-sensitive spin-label probe CTPO. J Magn Reson 1984;56:125–130.

53. Subczynski WK, Hyde JS. Diffusion of oxygen in water and hydrocarbons using an electron spin resonance spin-label technique. Biophys J 1984;45:743–748. [PubMed: 6326877]
54. Subczynski, WK.; Widomska, J.; Wisniewska, A.; Kusumi, A. Saturation-recovery electron paramagnetic resonance discrimination by oxygen transport (DOT) method for characterizing membrane domains. In: McIntosh, TJ., editor. Methods in Molecular Biology, vol 398: Lipid Rafts. Humana Press; Totowa: 2007. p. 145-159.
55. Marsh, D. Electron spin resonance: spin labels. In: Grell, E., editor. Membrane Spectroscopy. Springer-Verlag; Berlin: 1981. p. 51-142.
56. Gooden MM, Takemoto LJ, Rintoul DA. Evidence for reduced lipid order in plasma membranes from cataractous humans lenses. Curr Eye Res 1983;2:367–373. [PubMed: 7168959]
57. Li LK, Spector A, Cogan V, Schacter D. Dynamics of lipid fluorophors in bovine lens fiber membranes. Exp Eye Res 1982;34:145–151. [PubMed: 6895732]
58. Van Blitterswijk WJ, Van Hoeven RP, Van Der Meer BW. Lipid structural order parameters (reciprocal of fluidity) in biomembranes derived from steady state fluorescence depolarization measurements. Biochim Biophys Acta 1981;644:323–332. [PubMed: 7260077]
59. Puskin JS, Wiese MB. A spin label study of human lens membrane. Exp Eye Res 1982;35:251–258. [PubMed: 6288425]
60. Ferguson-Yankey SR, Borchman D, Taylor KG, DuPre DB, Yappert MC. Conformational studies of sphingolipids by NMR spectroscopy. I. Dihydrosphingomyelin. Biochim Biophys Acta 2000;1467:307–325. [PubMed: 11030590]
61. Talbott CM, Vorobyov I, Borchman D, Taylor KG, DuPre DB, Yappert MC. Conformational studies of sphingolipids by NMR spectroscopy. II. Dihydrosphingomyelin. Biochim Biophys Acta 2000;1467:326–337. [PubMed: 11030591]
62. Li L, Tang X, Taylor KG, DuPre DB, Borchman D, Yappert MC. Conformational characterization of ceramides by nuclear magnetic resonance spectroscopy. Biophys J 2002;82:2067–2080. [PubMed: 11916863]
63. Yappert MC, Borchman D. Sphingolipids in human lens membranes: an update on their composition and possible biological implication. Chem Phys Lipids 2004;129:1–20. [PubMed: 14998723]
64. Subczynski WK, Markowska E, Sielewiesiuk J. Spin-label studies on phosphatidylcholine-polar carotenoid membranes: effects of alkyl chain length and unsaturation. Biochim Biophys Acta 1993;1150:173–181. [PubMed: 8347671]
65. Subczynski WK, Markowska E, Gruszecki WI, Sielewiesiuk J. Effects of polar carotenoids on dimyristoylphosphatidylcholine membranes: spin-label studies. Biochim Biophys Acta 1992;1105:97–108. [PubMed: 1314674]
66. Pasenkiewicz-Gierula M, Subczynski WK, Kusumi A. Rotational diffusion of a sterol molecule in phosphatidylcholine-cholesterol membranes: fluid-phase microimmiscibility in unsaturated phosphatidylcholine-cholesterol membranes. Biochemistry 1990;29:4059–4069. [PubMed: 2163271]
67. Sankaram MS, Thompson TE. Modulation of phospholipid acyl chain order by cholesterol. A solid-state ^{2}H nuclear magnetic resonance study. Biochemistry 1990;29:10676–10684. [PubMed: 2271675]
68. Mitchell DC, Litman BJ. Effect of cholesterol on molecular order and dynamics in highly polyunsaturated phospholipids bilayers. Biophys J 1998;75:896–908. [PubMed: 9675190]
69. Langane B, Mazeres S, Le Grimellec C, Cezanne L, Lopez A. Lateral distribution of cholestrol in membranes probed by means of pyrene-labelled cholesterlo : effects of acyl chain unsaturation. Biophys Chemist 2002;95:7–22.
70. Subczynski WK, Wisniewska A. Physical properties of lipid bilayer membranes: relevance to membrane biological functions. Acta Biochim Polonica 2000;47:613–625.
71. McIntosh TJ. The effect of cholesterol on the structure of phosphatidylcholine bilayers. Biochim Biophys Acta 1978;513:43–58. [PubMed: 718889]
72. Seelig J, Waspa-Separovic N. Molecular order in *cis* and *trans* unsaturated phospholipids bilayers. Biochemistry 1978;17:3310–3315. [PubMed: 687586]
73. Wisniewska A, Subczynski WK. Accumulation of macular xanthophylls in unsaturated membrane domines. Free Radic Biol Med 2006;40:1820–1826. [PubMed: 16678020]

74. Wisniewska A, Subczynski WK. Distribution of macular xanthophylls between domains in model of photoreceptor outer segment membranes. Free Radic Biol Med 2006;41:1257–1265. [PubMed: 17015172]

75. Subczynski WK, Wisniewska A, Hyde JS, Kusumi A. Three-dimensional dynamic structure of the liquid-ordered domain in lipid membranes as examined by pulse-EPR oxygen probing. Biophys J 2007;92:1573–1584. [PubMed: 17142270]

76. de Almeida PFF, Pokorny A, Hinderliter A. Thermodynamics of membrane domains. Biochim Biophys Acta 2005;1720:1–13. [PubMed: 16472555]

77. de Almeida PFF, Federov A, Prieto M. Sphingomyelin/phosphatidylcholine/cholesterol phase diagram: boundaries and composition of lipid rafts. Biophys J 2003;85:2406–2416. [PubMed: 14507704]

78. Ge M, Gidwani A, Brown HA, Holowka D, Baird B, Freed JH. Ordered and disordered phases in plasma membranes of RBL-2H3 mast cells. An ESR study. Biophys J 2003;85:1278–1288. [PubMed: 12885671]

79. Epand RM, Maekawa S, Yip Ch M, Epand RF. Protein-induced formation of cholesterol-rich domains. Biochemistry 2001;40:10514–10521. [PubMed: 11523993]

80. Huang J, Buboltz JT, Feigenson GW. Maximum solubility of cholesterol in phosphatidylcholine and phosphatidylethanolamine bilayers. Biochim Biophys Acta 1999;1417:89–100. [PubMed: 10076038]

81. Cadenhead DA, Muller-Landau F. Molecular packing in steroid-lecithin monolayers part III: mixed films of 3-doxyl cholestane and 3-doxyl-17-hydroxyl-androstane with dipalmitoylphosphatidylcholine. Chem Phys Lipids 1979;25:329–343.

82. Presti FT, Chan SI. Cholesterol-phospholipid interaction in membranes. I. Cholesterol spin label study of phase behavior of cholesterol-phospholipid liposomes. Biochemistry 1982;21:3821–3830. [PubMed: 6291582]

83. Subczynski WK, Hyde JS, Kusumi A. Effect of alkyl chain unsaturation and cholesterol intercalation on oxygen transport in membranes: a pulse ESR spin labeling study. Biochemistry 1991;30:8578–8590. [PubMed: 1653601]

84. Subczynski WK, Markowska E, Sielewiesiuk J. Effect of polar carotenoids on the oxygen diffusion-concentration product in lipid bilayers. An EPR spin label study. Biochim Biophys Acta 1991;1068:68–72. [PubMed: 1654104]

85. Stockton GW, Smith IC. A deuterium nuclear magnetic resonance study of the condensing effect of cholesterol on egg phosphatidylcholine bilayer membranes . I. Perdeuterated fatty acid probes. Chem Phys Lipids 1976;17:251–263. [PubMed: 1033045]

86. Greenwood AI, Tristram-Nagle S, Nagle JF. Partial molecular volumes of lipids and cholesterol. Chem Phys Lipids 2006;143:1–10. [PubMed: 16737691]

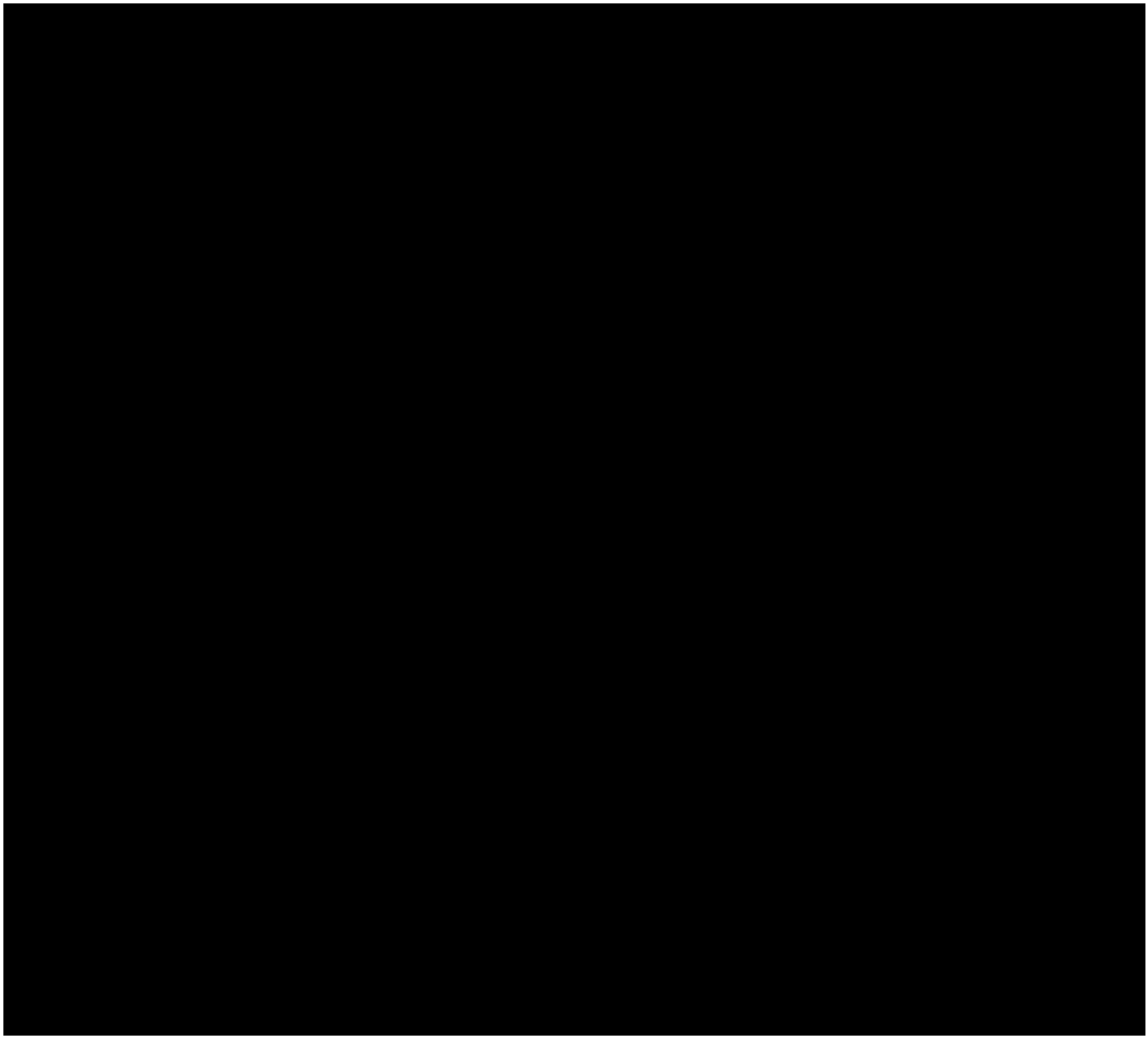

Fig 1.
Chemical structures of spin labels used in this work: n-PC, T-PC, 9-SASL, and ASL. Chemical structures of POPC and cholesterol molecules are indicated to illustrate approximate localization of these molecules and nitroxide moieties across the membrane.

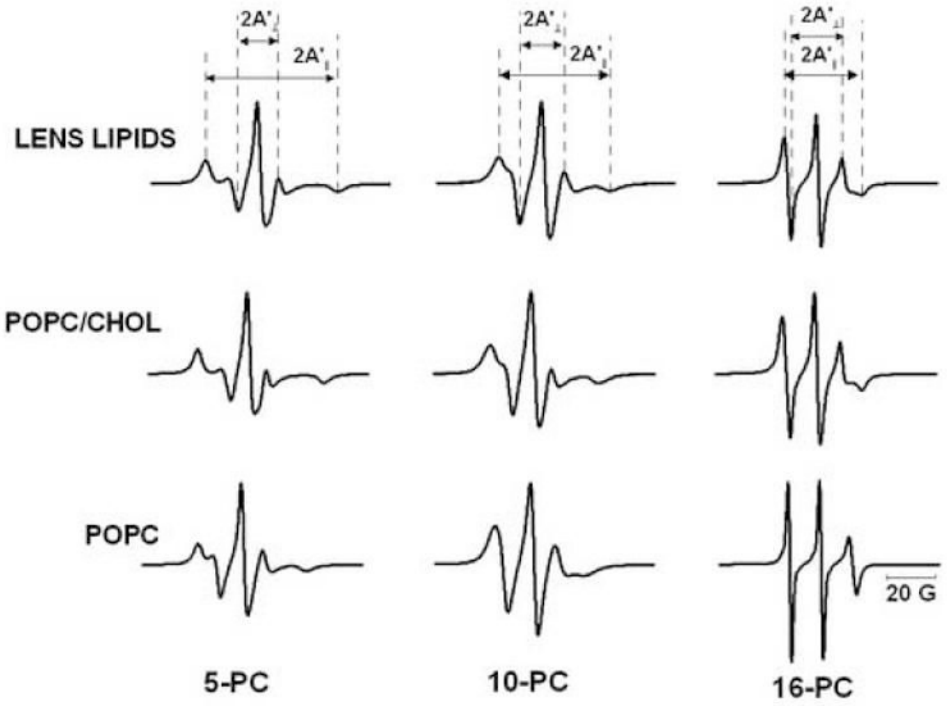

Fig 2.

Panel of EPR spectra of 5-, 10-, and 16-PC in membranes made of lens lipids, POPC/Chol equimolar mixture, and POPC. Spectra were recorded at 35°C. Measured values for evaluating the order parameter are indicated. The positions of certain peaks were evaluated with a high level of accuracy by recording them at 10-times higher receiver gain and, when necessary, at higher modulation amplitude.

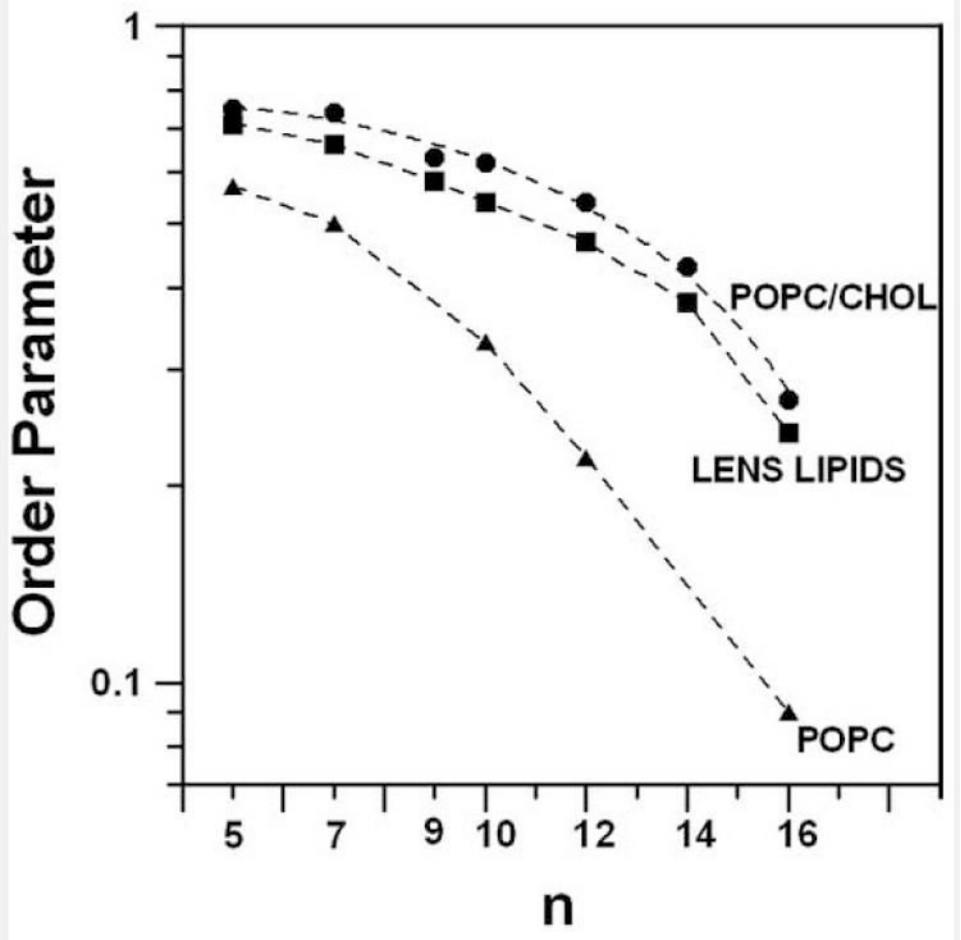

Fig 3.

Profiles of the molecular order parameter for membranes made of lens lipids, POPC/Chol equimolar mixture, and POPC (order parameter is plotted in a log scale as a function of nitroxide position (n) along the alkyl chain in spin labels) at 35°C. Points for pure POPC were taken from our previous work [30].

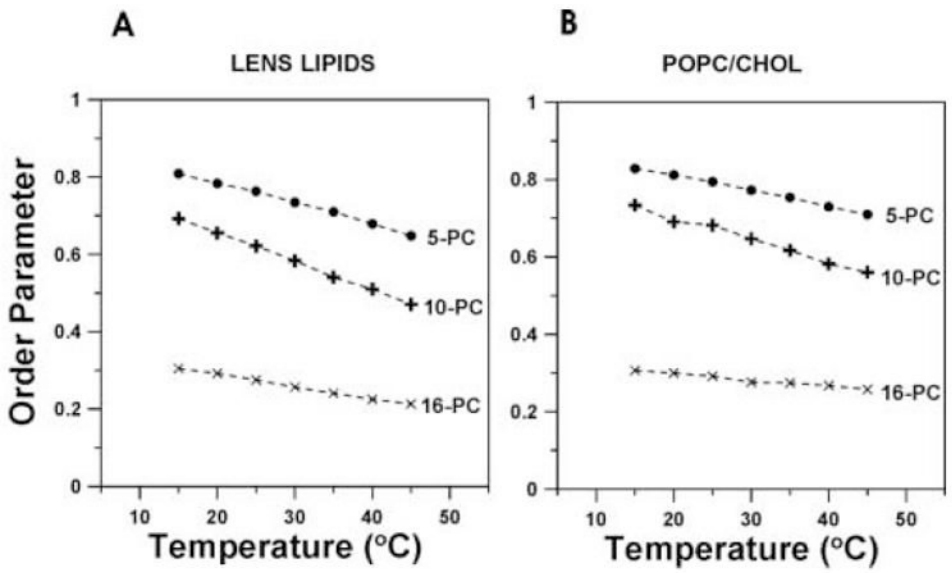

Fig 4.

Molecular order parameter of 5-, 10-, and 16-PC in membranes made of lens lipids (A) and POPC/Chol equimolar mixture (B) plotted as a function of temperature.

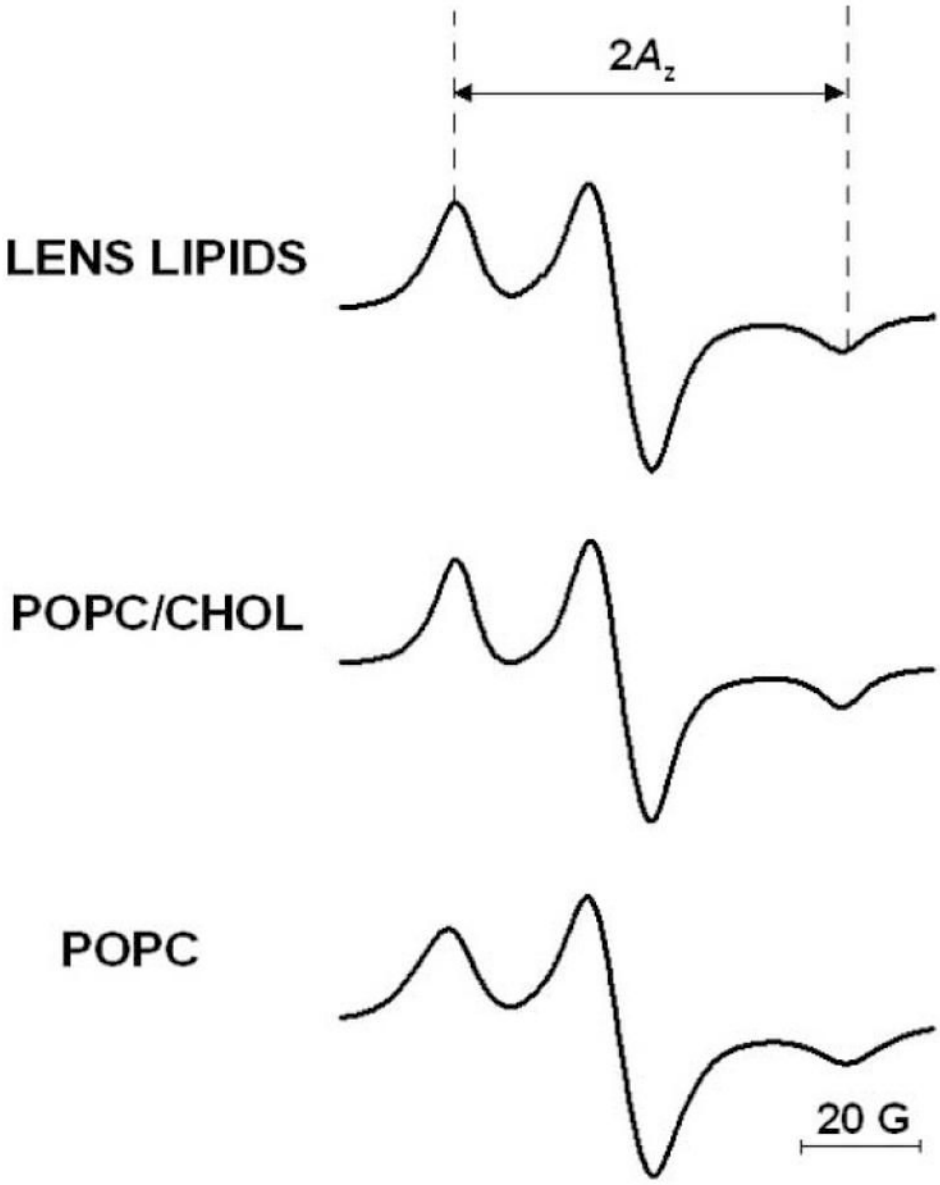

Fig 5.

EPR spectra of 14-PC in membranes made of lens lipids, POPC/Chol equimolar mixture, and POPC measured at −163°C. The measured $2A_z$ value (*z* component of hyperfine interaction tensor) is indicated.

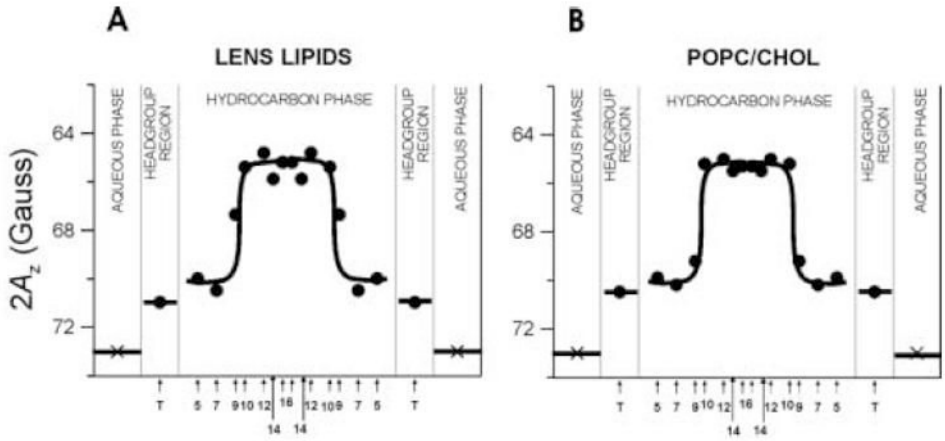

Fig 6.

Hydrophobicity profiles ($2A_z$) across membranes made of lens lipids (A) and POPC/Chol equimolar mixture (B). Upward changes indicate increases in hydrophobicity. $2A_z$ for 16-PC in the aqueous phase was calculated from the isotropic hyperfine constant of the nitroxide spin-label as shown in [40]. Because T-PC contains a different nitroxide moiety than n-PC and n-SASL, its points are not connected with other points. However, the relative changes of the hydrophobicity in the polar headgroup region can be evaluated. Approximate localizations of nitroxide moieties of spin labels are indicated by arrows.

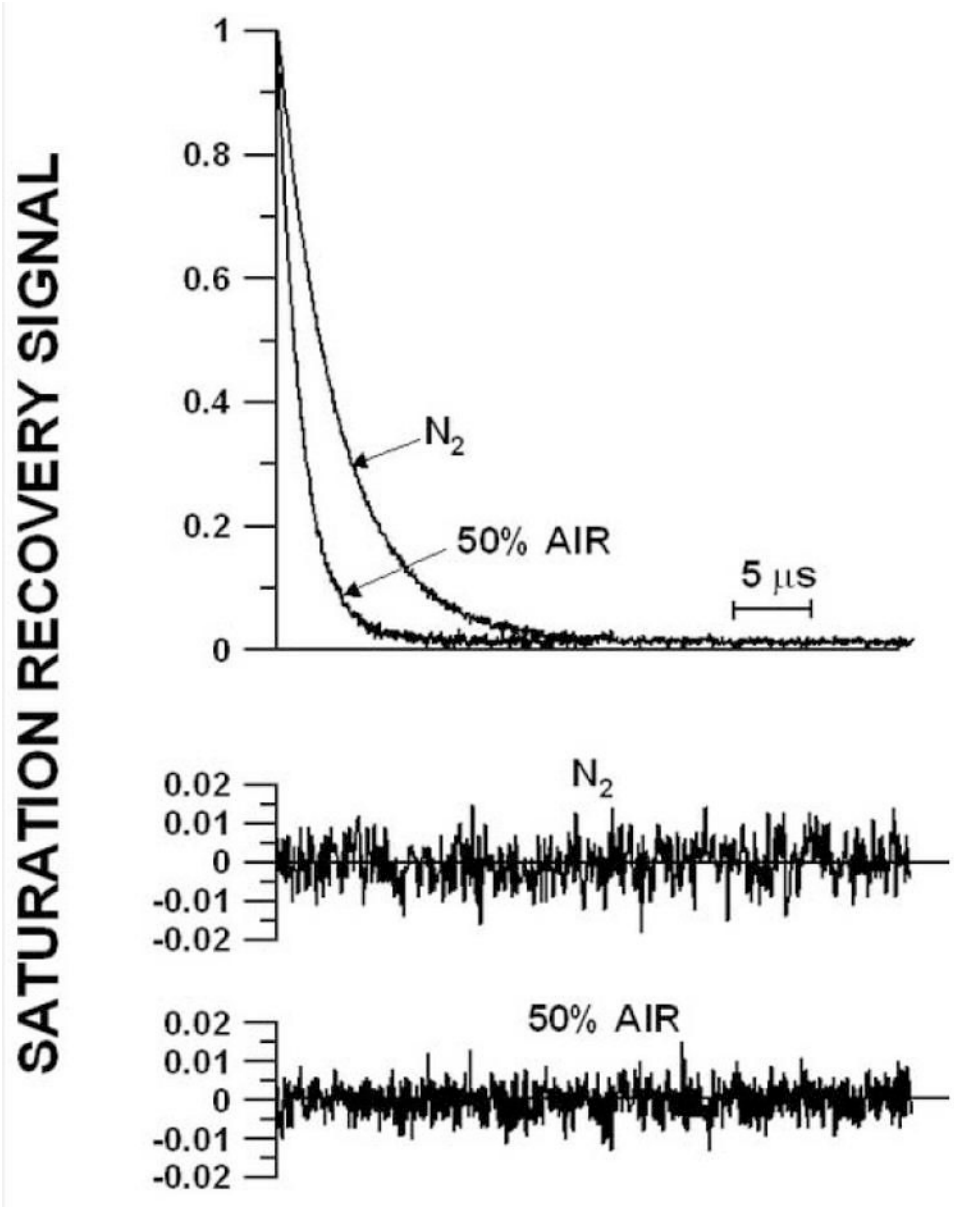

Fig 7.

Representative saturation-recovery signals and fitted curves of 5-PC in the membrane made of lens lipids at 35°C for the sample equilibrated with 100% nitrogen gas and with a gas mixture of 50% air and 50% nitrogen. The solid lines indicate the fit to single-exponential curves with recovery times of 1.6 μs (with 50% air) and 3.9 μs (with 0% air). The difference between the experimental data and the fitted curve is shown in the lower part of each recovery curve.

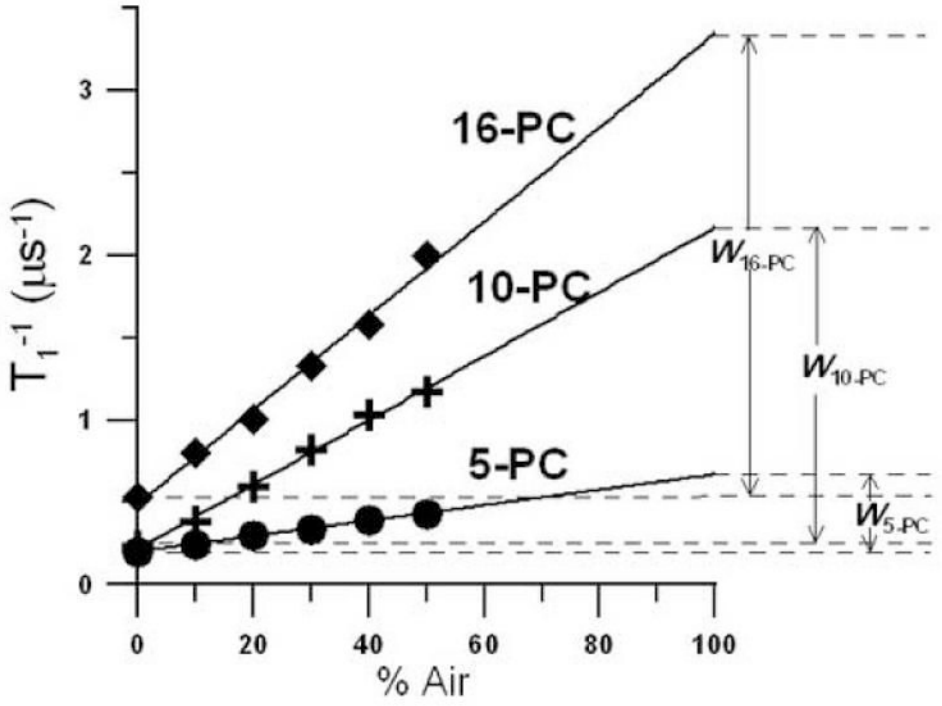

Fig 8.

T_1^{-1} for 5-, 10-, and 16-PC in the membrane made of lens lipids at 25°C plotted as % air in the equilibrating gas mixture. Experimental points show a linear dependence up to 50% air, and extrapolation to 100% air is performed to indicate a way of calculating oxygen transport parameters. $W_{5\text{-PC}}$, $W_{10\text{-PC}}$, and $W_{16\text{-PC}}$ are oxygen transport parameters measured for 5-, 10-, and 16-PC, respectively.

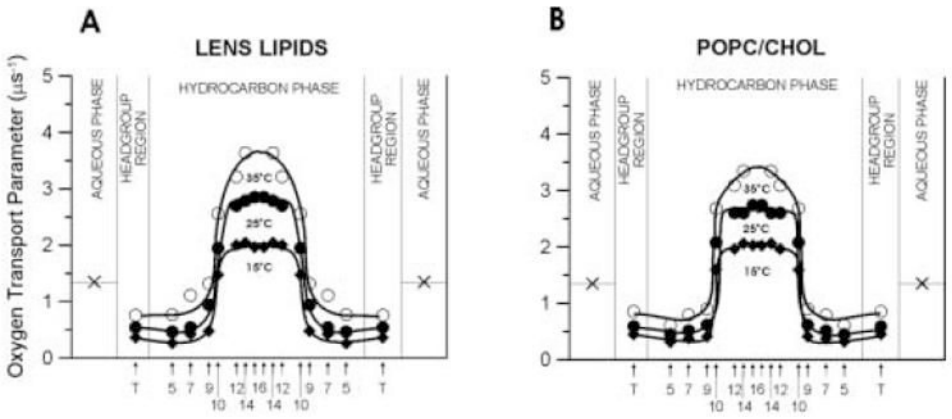

Fig 9.

Profiles of the oxygen transport parameter (oxygen diffusion-concentration product) across membranes made of lens lipids (A) and POPC/Chol equimolar mixture (B) obtained at 15 (♦), 25 (●), and 35°C (○). The symbol × indicates the oxygen transport parameter in the aqueous phase. It does not change significantly because temperature dependences of oxygen diffusion and concentration are opposite. Approximate localizations of nitroxide moieties of spin labels are indicated by arrows.

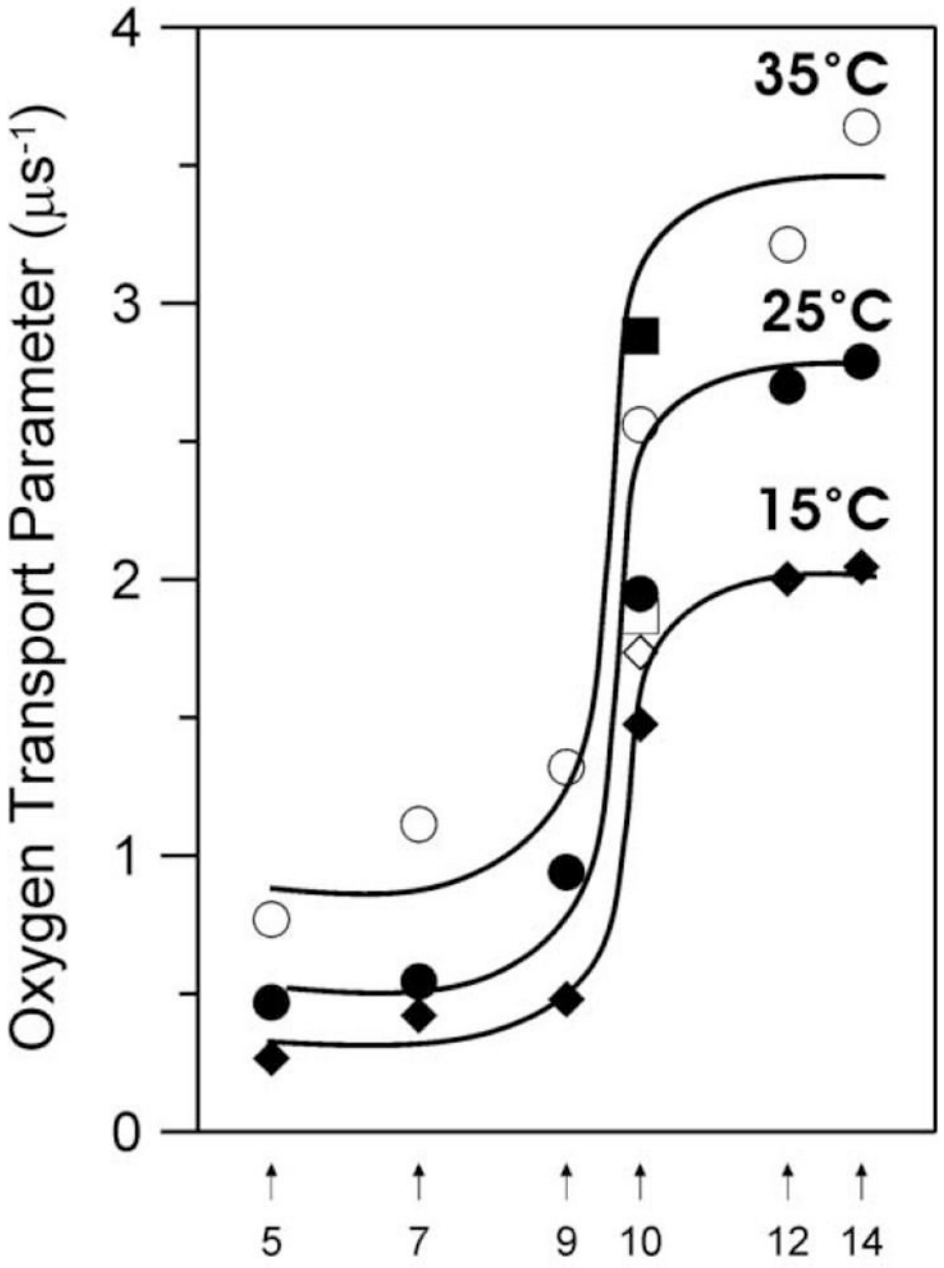

Fig 10.

The enlarged part of profiles of the oxygen transport parameter for the membrane made of lens lipids presented in Fig. 9A with added points for the cholesterol analogue spin label, ASL, at 15 (◊), 25 (□), and 35°C (■).